In Situ Surface Voltage Measurements of Dielectrics Under Electron Beam Irradiation

Joshua L. Hodges, JR Dennison, Justin Dekany,
Gregory Wilson, Amberly Evans, and Alec M. Sim

***Abstract*— New instrumentation has been developed for non-contact, *in vacuo* measurements of the electron beam-induced surface voltage as a function of time and position for non-conductive spacecraft materials in a simulated space environment. The novel compact system uses two movable capacitive sensor electrodes to measure surface charge distributions on samples, using a non-contact method that has little effect on charge dissipation from sample. Design details, calibration and characterization measurements of the system are presented, with <1 V to >30 kV surface voltage range, <0.5 V voltage resolution, and <1.5 mm spatial resolution. Used in conjunction with the capabilities of an existing ultrahigh vacuum electron emission test chamber, the new instrumentation facilitates measurements of charge accumulation, bulk resistivity, effects of charge depletion and accumulation on yield measurements, electron induced electrostatic breakdown potentials, radiation induced conductivity effects, and the radial dispersion of surface voltage.**

Three types of measurements of surface voltage for polyimide (Kapton HN™) serve to illustrate the research capabilities of the new system: (i) accumulation using a pulsed electron beam, while periodically measuring the surface voltage; (ii) post charging, as deposited charge dissipated to a grounded substrate; and (iii). the evolution of spatial profile resulting from an incident Gaussian beam. Theoretical models for sample charging and discharge are outlined to predict the time, temperature, and electric field dependence of the sample's net surface voltage.

***Index Terms*—Surface charging, surface discharge, electrostatic discharge, materials testing, polyimide films, pulsed beams, test facilities, space environment interactions**

I. Introduction

Surface charging and subsequent electrostatic discharge due to interactions with the space environment is one of the primary concerns of spacecraft charging studies [1-4]. Laboratory measurements of the evolution of surface voltages and dissipation currents under simulated space conditions are the primary method used to determine the response of key materials to diverse incident fluxes.

This paper describes the design and use of a system to measure the accumulation and dissipation of surface charge on an insulator as a function of time and position *in situ* in a spacecraft charging vacuum test chamber. Surface charge is generated by incident fluxes that deposit charge and energy near the surface, and create secondary and backscattered electrons which are emitted from the material. The low charge mobility of insulators causes charge to accumulate where deposited, preventing even redistribution of charge and creating inhomogeneous local electric fields and potentials across the material; this drives charge transport and can lead to electrostatic breakdown. Deposited charge dissipates on relatively long time scales by charge transport through highly resistive materials to grounded substrates. The conductivity of the material is a key transport parameter in determining how deposited charge will distribute across the spacecraft, how rapidly charge imbalances will dissipate, and what equilibrium potential will be established under given environmental conditions [1,5-6]. Hence, it is critical for reliable spacecraft charging models to use appropriate values of conductivity for thin film insulators to determine the correct charge distributions and charge storage decay times for the materials.

The bulk conductivity values of commonly used insulators have most often been determined using standard ASTM methods [7], with a parallel plate capacitor geometry and a voltage applied with electrodes (see Figure 1(a)). Similar tests have been done under vacuum conditions which are more analogous to space environments [8]. However, in many cases the charge storage method using surface voltage measurements [5,8-11] can measure lower conductivity values and is more similar to situations encountered in spacecraft charging [5,9,11]. Charge decay methods expose one side of the insulator in vacuum to incident charged particles, light or plasma, with a conductive electrode attached to the other side of the insulator. Data are obtained by capacitive coupling to measure both the resulting voltage on the open surface and emission of electrons from the exposed surface, as well monitoring both conductive and displacement currents to the electrode (Figure 1(b)). In many space applications, the upper surface of the exposed insulator is floating and there is no electric field applied by electrodes but rather only electric field from self-charge.

The general design parameters of the system are set by the extent of the spacecraft charging problem [12]. A desired lower voltage range and voltage resolution is $\lesssim$1 V. This is

Research was supported by funding from the NASA James Webb Space Telescope project at the Goddard Space Flight Center and support from the US Air Force through the PALACE Acquire Program.

Joshua Hodges is Service Life Monitoring Program Manager with the Mature and Proven Aircraft Division, Hill Air Force Base in Ogden, UT 84056 USA (e-mail: Joshua.Hodges@hill.af.mil. JR Dennison is a professor with the Materials Physics Group in the Physics Department at Utah State University in Logan, UT 84322 USA (e-mail: JR.Dennison@usu.edu). Justin Dekany, Gregory Wilson and Amberly Evans are graduate students in the Materials Physics Group. Alec Sim is an Assistant Professor in the Department of Physical Sciences at Irvine Valley College, Irvine CA 92618 USA (e-mail: ASim@ivc.edu).

Color versions of one or more figures in this paper are available online at http://ieeexplore.ieee.org.

Digital object identifier .

estimated as ~10% of the electrostatic breakdown potential for thin film sample such as oxide layers or dielectric coating on the order of 10^{-6} to 10^{-5} m thick with typical electrostatic field strengths of 10^{7} to 10^{8} V/m and breakdown voltages of 10^{1} to 10^{3} V. A desired upper voltage range is ≳30 kV [13]. This is the upper bound on incident electrons that most affect surface charging events [14], is also an upper bound on surface charging beyond which electrons penetrate far enough into materials that electron emission is minimal [15], and is the typical breakdown voltage for common ~100 μm thick blanket materials. Desired instrument response times can be estimated from dissipation times for low conductivity materials (10^{-12} $(\Omega\text{-cm})^{-1}$ to 10^{-20} $(\Omega\text{-cm})^{-1}$)—with corresponding dissipation times of a few times 10^{-1} s to 10^{7} s—identified as problematic in spacecraft charging [16]. This suggests a response time on the order of 1 s is appropriate and a system stable over a few days would be required to see a few percent decay in the lowest conductivity materials [12]. Spatial resolution on the order of a few mm is also desirable, to facilitate monitoring lateral charge movement in dielectric samples on the length scale of a typical incident beam diameter.

The instrumentation is briefly described here, emphasizing how the sensor is incorporated into an existing detector. More extensive descriptions of the instrumentation and calibration—including the surface voltage probe (SVP) and electrostatic field transfer probe (EFTP)—are found in [12] and [17]. Three measurements are described to illustrate the research capabilities of the test system. Surface voltage measurements were made periodically during the electron beam charging process and as the surface voltage discharged to a grounded substrate after exposure. Analysis of the measured curves provides information about the material electron yields and bulk resistivity. The evolution of the spatial profile of the voltage across the sample surface was also measured by sweeping a small electrode across the surface.

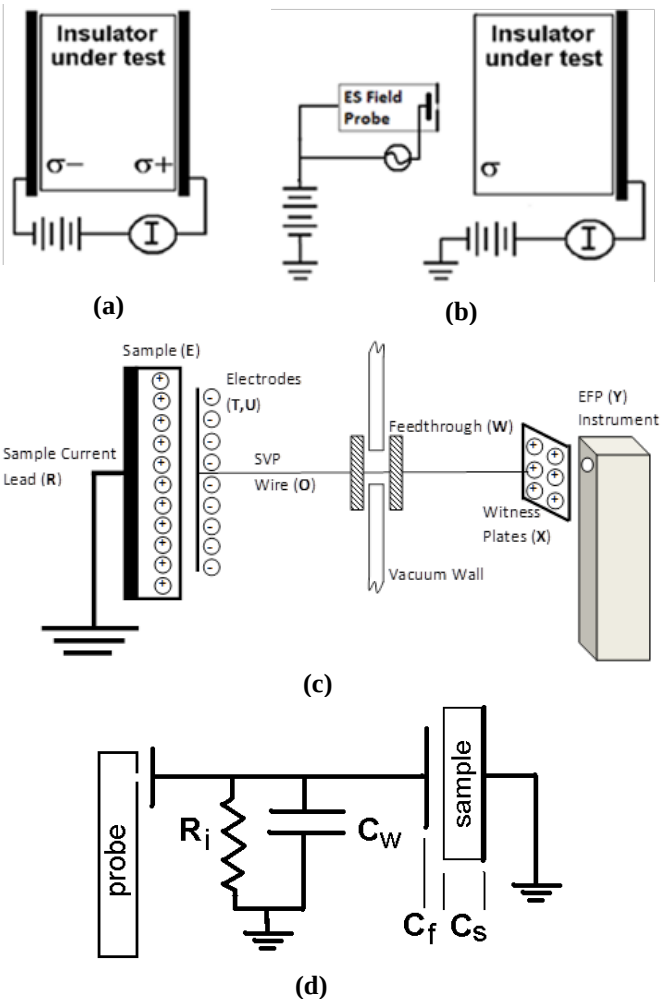

Fig. 1. Schematics of the electrostatic field probe (EFTP) assembly. *Schematic representation for two different types of resistivity measurements:* (a) *classical electrode method and* (b) *charge storage method.* (c) *Charge distribution for the EFTP assembly. Shown are the sample (left), EFTP (center), and electrostatic field probe, (right). (d) Effective circuit for EFTP.*

II. INSTRUMENTATION

Our novel surface voltage probe system is shown below to meet the general design guidelines for measurements most relevant to spacecraft charging issues. The response time of the probe and data acquisition system are fast enough to acquire data for lower resistivity materials such as low density polyethylene (LDPE), with a few seconds decay times. The long term stability and drift characterization required to measure at slow rates and take data over several days on materials that have a high resistivity like Kapton™ necessitate computer controlled data acquisition.

Design details, calibration and characterization measurements are presented for a system that meets the general design goals outlined above. The compact system uses two movable capacitive sensor electrodes (3 mm and 7 mm diameter) that can be swept across the sample using an *in vacuo* stepper motor to measure surface charge distributions on samples *in situ*, using non-contact electrostatic field probe methods that does not dissipate significant sample charge.

A. Overview of Electron Emission Test Chamber

The compact transfer probe design extends our measurement capabilities by allowing the surface voltage probe to fit within an existing hemispherical grid retarding field analyzer, so that surface voltages can be measured on samples tested using the extensive source flux and emission detection capabilities of an existing electron emission vacuum test chamber. An overview of the main electron emission test chamber is included to illustrate the full capabilities of the surface voltage test system. Further descriptions of this versatile ultrahigh vacuum (UHV) chamber are provided elsewhere [4,17-23] This chamber can simulate diverse space environments including controllable vacuum ($<10^{-10}$ to 10^{-3} Torr) and ambient neutral gases conditions, temperature (<40 to >400 K), as well as sources for a broad range of electron, ion and photon fluxes and energies.

Two primary electron sources provide monoenergetic electron beams ($\Delta E/E<2\bullet10^{-4}$) with electron energy ranges from ~20 eV to ~30 keV, beam spot full width at half maximum (FWHM) ranging from ~50 μm to >100 mm (depending on beam energy), and pulsing capabilities ranging from 10 ns to dc emission. Stable, uniform, well-characterized beam fluxes of 0.05 nA-cm^{-2} to >1 μA-cm^{-2} are possible from the electron guns. There are three ion guns with <0.1 to 5 keV monoenergetic sources for inert and reactive

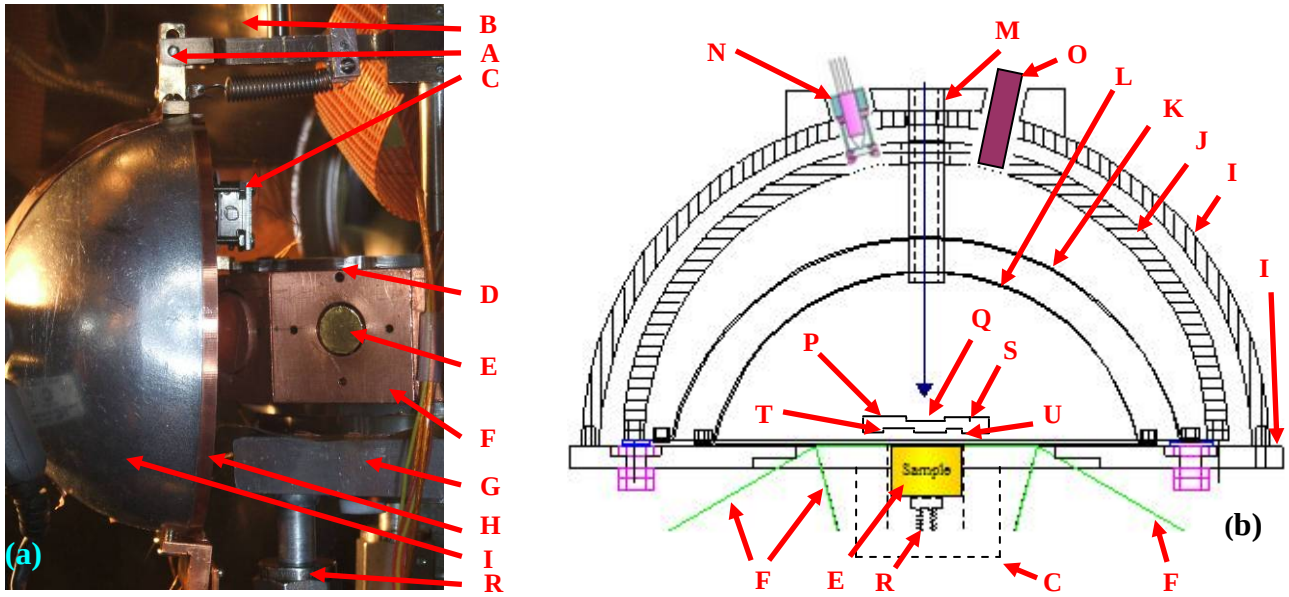

Fig. 2. Hemispherical Grid Retarding Field Analyzer (HGRFA). *(a) Photograph of sample stage and HGRFA detector (side view). (b) HGRFA cross section.*

LEGEND

A *HGRFA Hinged Mount*	***I*** *HGRFA Hemispherical Shield*	***R*** *Sample Current Lead*
B *Sample Carousel/HGRFA Rotation Shaft*	***J*** *HGRFA Collector*	***S*** *SVP Faraday Cup*
	K *HGRFA Bias Grid*	***T*** *SVP 7 mm Diameter Au Electrode*
C *UHV Stepper Motor*	***L*** *HGRFA Inner Grid*	***U*** *SVP 3 mm Diameter Au Electrode*
D *Sample Block Faraday Cup*	***M*** *HGRFA Drift Tube*	***V*** *SVP Wiring Channel*
E *Sample (10 mm)*	***N*** *Electron Flood Gun*	***W*** *EFTP Vacuum Feedthrough*
F *Sample Block*	***O*** *LED Light Source*	***X*** *EFTP Witness Plate*
G *Cryogen Reservoir*	***P*** *Surface Voltage Probe (SVP)*	***Y*** *Electrostatic Field Probe*
H *HGRFA Face Plate*	***Q*** *Au Electron Emission Standard*	***Z*** *Probe XYZ Translator*

gases. The NIR-VIS-UV solar irradiance spectrum is simulated using a pair of pulsed, monochromated tungsten/halogen and deuterium RF powered continuum lamp sources produce focused (~0.5 cm diameter) radiation from 0.4 eV to 8.3 eV (150 nm to 2000 nm). Additional light sources include a Kr resonance lamp (10.3 eV), broadband Hg discharge and W-filament sources, and a variety of quasi-monochromatic NIR/VIS/UVA LED sources [4].

For conducting samples, electron guns are operated using a continuous, low-current beam of electrons, and dc-currents are measured with standard ammeters sensitive to $\lesssim 10^{-13}$ A. The system at USU to measure electron emission from insulators uses a combination of methods to control the deposition and neutralization of charge. Typically, charge deposition is minimized by using a low current beam (~10-30 nA) focused on a sample area of ~7 mm^2 that is delivered in short pulses of ~5 μsec (~150 fC or ~10^5 electrons-mm^{-2} per pulse). For a typical ~100 μm thick dielectric sample, this amount of charge is estimated to change the surface potential by only 10-100 mV/pulse (positive) and requires ~500 pulses/sec to achieve an ~1 nA/cm^2 dosage that typically causes discharge in space. The pulsed system uses custom detection electronics with fast (1-2 μs rise time) sensitive/low noise (10^7 V/A /100 pA noise level) ammeters [20,21]. Detected current pulses are sent to a fast (1 GS/s) digital storage oscilloscope, equipped with resistive and induction sensors. Charge dissipation techniques include a custom low energy (~1-10 eV) electron flood gun for direct neutralization of positively charged surfaces between incident pulses [20,21,24] and use of visible and UV light sources for neutralization of negatively charged surfaces through the photoelectric effect. Sample heating to ~50-100 °C has also been used for dissipation of buried charge by thermally increasing the sample conductivity. Both DC and pulsed measurements and data retrieval are fully computer automated under LabVIEW^{TM} control. A complete description of the DC-system and pulsed-system setups is provided in [18-21], along with additional insulator-yield and charging data.

B. Detector Assembly

A variety of detectors are available for measurements of single or simultaneous electron-, ion-, and photon-induced emission [18,20,21], including a standard Faraday cup detector, hemispherical analyzer, cylindrical mirror analyzer, and time of flight microchannel plate detector. Specifically, these allow us to measure total emitted electron (ion and photon) yield, backscattered/secondary yield, charge decay curves, and emission energy spectra [12].

The primary detector for emission studies is a custom hemispherical grid retarding field analyzer (HGRFA), with a retarding-field analyzer grid system for emitted-electron energy discrimination between back scattered electrons (energies >50 eV) and secondary electrons (energies <50 eV) (see Fig. 2). By ramping the grid (refer to labels **K** and **L** in Fig. 2) bias, energy spectra of the emitted electrons can also be measured using this detector. The HGRFA features an

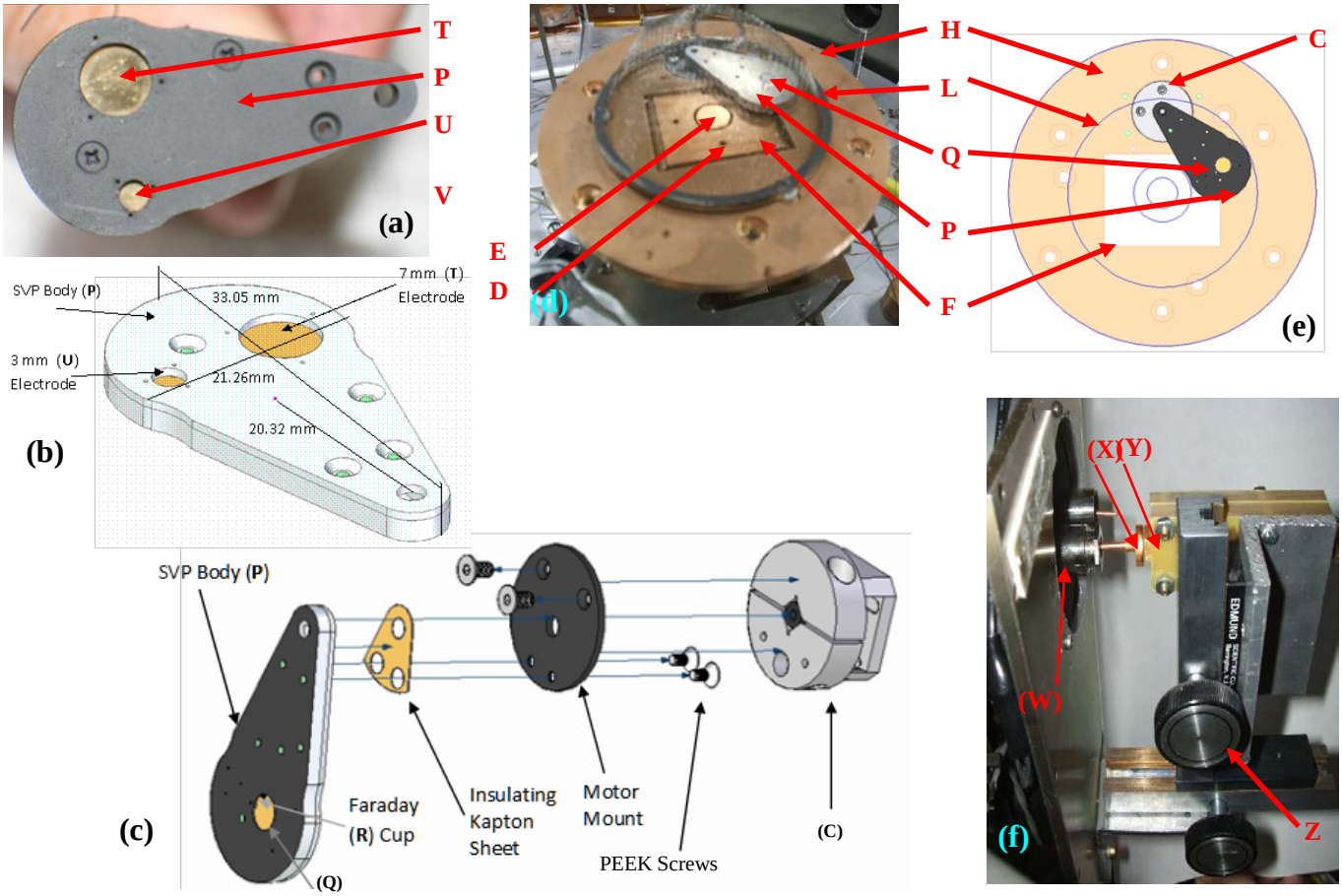

Fig. 3. Surface Voltage Probe (SVP). *(a) Photograph of sample side of SVP assembly. (b) Overall dimensions of SVP with center of gravity indicated. (c) Exploded view of SVP parts and SVP motor assembly. (d) Photograph of the SVP, mounted on the HGRFA, with the collecting hemisphere removed. (e) Diagram of HGRFA interior with SVP, looking toward the sample. (f) 6 axis EFP translation stage mounted parallel to a witness plate.*

aperture and drift tube (**M**) for incident electron/ion admission and a fully-encasing hemispherical collector (**J**) for full capture of emitted electrons, that is particularly well suited and calibrated for absolute yield measurements [18,19,21]. The HGRFA detection system has been carefully calibrated to account for detector losses, allowing yield accuracies of better than 2% for conductor yields and 5% for insulator yields [4,17,18]. The HGRFA can be independently positioned in front of any sample (**E**) (see Fig. 2(a)). A low energy flood gun (**N**) and a variety of visible and UV LED light sources (**O**) are mounted on the HGFRA housing at near-normal incidence to provide neutralization of surface charging between pulses. A collimating lens mounted on the HRFA and attached to a fiber optic cable and vacuum feedthrough allow external light sources to be used or a photospectrometer to analyze emitted light from the sample. The flood gun (**N**) also acts as a low energy (~1eV to 100 eV) focused electron source.

C. Sample Assembly

Samples (**E**) are typically mounted on (10.0 ± 0.1) mm diameter Cu cylinders [17]; sample up to 26 mm diameter can be accommodated. The Cu cylinders are mounted in sample blocks (**F**) on the sample carousel, and are electrically isolated. Electrical connection to the sample is made via one or more spring loaded pins (**R**) from the rear, allowing the current(s) to the sample to be monitored. The primary sample carousel is a right dodecagon that has eleven sample blocks that can be rotated in front of the various flux sources (see Figs. 2(c-e) in [17]). Typically, one sample block contains a photodiode, another a Faraday cup, and a third a Au sample as an electron emission standard. The sample carousel can be easily removed for rapid sample exchange and is mechanically positioned relative to the HGRFA face plate within ±0.5 mm. *Ex situ* tests showed no significant changes in the calibration factors for changes in probe to sample distances <5 mm.

The sample carousel is mounted on a cryogenic reservoir; it is electrically isolated using a ~75 μm thick Chotherm™ sheet that provides good thermal contact. Liquid nitrogen cooling allows sample temperatures maintained to within ±5 K. Temperatures ≳400 K can be achieved using resistive heating elements, held to within ± 1 K. The large thermal mass of the sample stage helps minimize temperature fluctuations. An alternative low-temperature sample stage has been developed for use with the HGRFA/SVP assembly [25]. The sample holder uses a closed cycle He cryostat to attain sample temperatures from ≲40 K to >350 K, with ≲0.5 K stability maintained by a standard PID temperature controller.

D. Surface Voltage Probe Design

The surface voltage probe (SVP) is a small device that fits within the HGRFA to measure the surface potential of a sample. Extensive details of the SVP system are given in [12] and [17] and a block diagram of the SVP system and electronics is shown in Figure 4 of [17]. Figure 3(c) shows the assembled SVP, which is <40 mm long and only ~21 mm wide, with a thickness of <3 mm. Two openings in the casing

of 7.0 mm (**T**) and 3.0 mm (**U**) diameter define the effective electrode areas. The casing is coated with colloidal graphite to minimize the production of secondary electrons by stray electrons inside the HGRFA (see Fig. 3(a)). There are two electrodes (**U** and **T**) on the sample side of the sensor ~500 µm above the sample surface, each kinematically positioned and electrically isolated by six 500 µm diameter sapphire spheres above and below the electrodes. The electrodes are Au plated to minimize surface contamination and allow a uniform charge density on the probe. Currents to the two electrodes, the Au disc, and the full SVP casing can be monitored independently because each are electrically isolated. The two voltage sensor plates are connected separately to external witness plates (**X**).

The SVP is mounted on a small sized (~25 mm x 11 mm diameter), ultrahigh vacuum-compatible stepper motor (Attocube Systems, Model ANR50res) (**C**). The microstepper controller (Model ANC200), with a resistive position encoder, provides rapid and extremely fine (<1 m° per step) positioning. The SVP can be positioned on either side of the sample providing an unobscured view for the incident beam and can be swept from side to side allowing either electrode to pass fully over the sample.

The SVP is a much smaller detector than commercial electrostatic field probes; this allows the SVP to be incorporated within the HGRFA (see Figs. 3(d) and 3(e)). The primary advantage positioning the SVP inside the HGRFA is that surface voltage measurements can be made rapidly, while the sample and HGRFA are accurately aligned with the incident beam. In addition, an electrically isolated 4.15 mm diameter Au disc (**O**) is mounted on the source side of the probe and can be swung into place above the sample in line with an incident beam, providing a Au electron emission calibration standard for the detector [21,26,27]. Further, the SVP in this position can act as a shield for the sample preventing any stray electrons or light from charging or discharging the sample. There is also a 360 µm diameter Faraday cup (**S**) in the source side of the probe that can be swept across the sample to center the beam on the sample.

E. Electrostatic Field Transfer Probe Design

The EFTP used here is based on Frederickson's idea that a transfer probe can induce a surface voltage on an external witness plate proportional sample surface voltage, that can be easily measurable outside of the vacuum [5,28]. The EFTP (see Fig. 1 (c) and Fig. 3) consists of one of the surface voltage probe electrodes (**U** or **T**) positioned above the sample connected to an external witness plate (**X**) by ~1 m of thin 152 µm diameter 36AWG manganin wire (Lakeshore, Part WSL-32-100) with very thin polyvinyl formal (Formvar®) insulation to minimize the capacitance of the EFTP. Each electrode is connected to a 4 mm x 15 mm diameter polished Au-plated external witness plate (**X**) mounted to an ultrahigh high vacuum compatible dual floating MHV feedthrough (**W**) positioned outside the vacuum chamber close to a standard electrostatic field probe (**Y**). The sensor of the electrostatic field probe (Monroe Electronics Isoprobe, Model 162) (**Y**) is mounted on a precision XYZ translation stage (**Z**) to position the probe in front of one or the other witness plates with a ~0.5 mm probe-to-plate separation. The electrostatic field probe control electronics (Monroe Electronics, Model 1017AEL) can measure surface voltage of ±10 V with a resolution of ±1 mV. Provisions have been made to alternately mount another electrostatic field probe (Trek, Model 341 A) that can measure surface voltages of ±20 kV with ~0.5 V resolution to measure higher sample voltages. The probes and witness plates are mounted in a metal enclosure that provides electrostatic shielding and allows purging of the enclosure with dry nitrogen to reduce leakage voltages across the plate gaps due to moist air.

There are distinct advantages in using the EFTP and having the electrostatic field probe outside the vacuum chamber. Others have measured the surface voltage directly with electrostatic field probes inside the vacuum chamber and adjacent to the sample [9,29]; however, these methods were often subject to problems [30,31]. The required proximity of the electrostatic probe to the sample means that stray electron beam radiation—from secondary scattering, insufficient beam columniation, or beam rastering—can charge the sensitive electrostatic probe, often driving it off scale. It is difficult to discharge a probe in vacuum; this can lead to large, unpredictable and persistent voltage offsets and can even damage the probe that cannot be readily repaired *in vacuo*.

III. CALIBRATION AND MEASURMENTS

A. Measurement and Calibration Principles

To accurately measure a surface voltage with the EFTP, the sample plate and witness plate are positioned adjacent to grounded surfaces and the EFTP is grounded. This assures that there is no net charge on the EFTP and that the charge density is zero on both plates. The EFTP is then disconnected from ground and the witness plate voltage is measured with the electrostatic field probe; this provides a measure of the zero offset V_{offset}, which is the measured probe voltage for a grounded sample. A known voltage is then placed on a conducting sample, causing an equal magnitude and opposite polarity charge density to form on the voltage sensor plate. However, since the EFTP still has no net charge (assuming the probe is fully isolated), an equal magnitude charge is found at the opposite end of the EFTP. The charge density on the witness plate, σ_w, is then of the same polarity as the sample charge density, σ_s, with magnitude of the witness plate charge density scaled by the ratio of the voltage sensor plate to witness plate capacitances, $\sigma_w=(C_f\ /C_{WP})\sigma_s \equiv CF \bullet \sigma_s$. The proportionality constant, *CF*, depends on the plate areas and separations, but can be determined directly by measuring the witness plate voltage with the external electrostatic field probe for a variety of applied sample voltages. Typical calibration errors for the system are shown in Fig. 5 of [17], and further details of the calibration process are given in [12]. Once calibrated, the EFTP can then be used to measure unknown surface voltages or charge densities of conducting or insulating samples.

In an ideal system, the probe has infinite resistance and zero capacitance coupling to ground. More correctly, one must consider the coupling of the EFTP to ground, including both the capacitance of the wire and probes and the leakage resistance to ground through the feedthrough, wire insulation, and probe mounts [30]. An expression for the time-dependant voltage on the sample, V_s,

$$V_s = \left(\frac{C_W + C_f}{C_f}\right) V_{probe_o} e^{-t/\tau} \qquad with \quad \tau = R_i C_W \qquad (1)$$

uses an exponential decay of the initial probe voltage V_{probe_o} with time as charge leaks into (or from) the EFTP, with an RC time constant, τ (see details in [12] and [17]). The three largest sources of a resistance for R_i are the leakage through air of the witness plate to the EFTP (~4•10^{14} Ω), the electrical isolation of the electrodes to the probe body through the sapphire spheres (~3•10^{14} Ω), and the vacuum feedthrough to ground (~1•10^{14} Ω). The highest sources of capacitance of the probe, C_w, are the capacitance of the feedthrough (~12 pF) and the capacitance of the wire (~6 pF).

Another reason for preferring the EFTP arrangement relates to electron emission from insulators [5]. Electron beam charging of the samples produces an electric field at the surface of the sample that can drive electrons out of the surface. While penetrating into the insulator, the high-energy electrons excite electrons and holes into trapping states and into mobile states located in the region between the sample surface and the maximum depth of penetration. Such trapped charge provides the charge to be later emitted from the surface. This effect is sometimes termed the Malter effect [28,32]. An *in situ* electrostatic field probe can collect these delayed emitted electrons, thereby altering the net charge on the electrostatic field probe and modifying the voltage reading with time. The same modification of the net charge on the EFTP can occur for *ex situ* electrostatic field probes. However, by knowing the sample surface plate to voltage sensor plate capacitance, C_f, the rate of voltage change on the voltage sensor plate provides a direct, sensitive determination of the electron currents leaving the sample surface. [12] and [17] describe a calibration method to account for this effect.

B. Calibration

To determine the calibration factor of the EFTP, measurements were made of the probe voltage for a series of known sample voltages. The large electrode has a repeatable calibration factor of CF=1084.5±0.5 V_p/V_s over a range of applied voltages >1000 V. It is good practice to determine the calibration factor for each set of experiments as well, as there is some small variation due to specific sample and sensor conditions and sample-to-sensor separation. The calibration factor was approximately proportional to this separation, as expected for the parallel plate geometry; however, this separation was quick reproducible for a given sample and variations from one sample to the next were accounted for by measuring a calibration factor for each sample. Tests also indicated that an accurate surface voltage measurement could be made in <500 ms, as limited by the time constant of the EFTP (~100 ms), the response time of electrostatic field probe (<5 ms), and data acquisition time.

The probe offset voltage (typically on the order of a few mV) and voltage drift with time were found to differ for each test and must be measured for each test sequence by performing an applied voltage calibration run. To calibrate the EFTP drift due to leakage, a constant voltage was applied to the sample and the probe voltage was monitored with time over ~2 hr. At a zero applied voltage, the probe voltage was found to change almost linearly with time over early times at a rate of (V_{drift_o}/τ_D)=280 μV/s. Measurements made for nonzero applied voltages produced very similar drift rates. Without correcting for voltage drift, there would be a ~0.5 V error in measured surface voltage, comparable to the instrument resolution, in ~12 s. After correcting for a linear drift, measurements can be taken for > 4 hr with <20 V error.

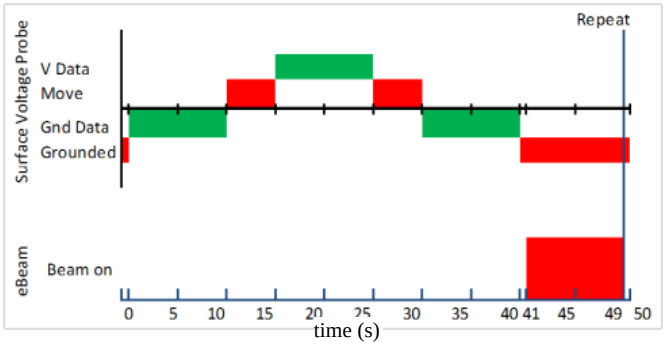

Fig. 4. Timing of a typical charge accumulation/dissipation run. Green represents time at which data are being collected. Grounded times varied depending on the "beam on" time.

Hodges provides a much more detailed discussion of the calibration that becomes relevant for operation of the SVP requiring higher precision or longer times between recalibration [12]. His calibration extends the linear approximation for drift in Eq. 2 to an exponential correction as expressed in Eq. 1 and additional corrections for the drift in the detector electronics and exponential drifts in time and voltage of the sample voltage.

Combining the results of the calibration tests, the measured probe voltage is related to the actual surface voltage through a linear approximation to Eq. 1 as:

$$V_s(t) = CF\left[V_{probe_o}\left(1+\frac{\beta}{\tau_v}(t-t_v)\right) - V_{offset} + \frac{V_{drift_o}}{\tau_d}(t-t_d)\right] \qquad (2)$$

where $(t-t_d)$ and $(t-t_v)$ are the elapsed time since recalibration of the probe to a grounded surface and the time that the probe has been positioned over a sample, respectively. For times ≲150 s voltage drift is negligible (*i.e.*, $\beta \rightarrow 0$) and a linear approximation for the temporal drift introduced errors less than other sources of error. The EFTP and SVP assembly was sensitive to a surface voltage of <1 V with a resolution of ~0.5 V. Surface voltages up to ±12 kV could be measured with the Monroe probe. Much higher voltages (in principle up to ±30 kV) could be measured with a Trek electrostatic field probe. A modest voltage drift rate was observed in the sample voltage of <3 mV_s/sec. Without correction for drift, surface voltages can be measured for short periods of time—long enough for accurate surface sweeps—between recalibration of the probe. With a linear voltage drift correction, surface voltages can be measured to high accuracy for periods >4 hr between probe recalibration.

Data were acquired and processed using an automated Labview™ program. The SVP data are typically sampled at 1 kHz for 1 s intervals; averages and standard deviations are retained. Figure 4 shows a typical timing diagram for data acquisition. 10 s of data with the SVP positioned over a grounded plane are acquired before and after a 10 s interval of data acquired with the SVP positioned over the sample; V_{offset} and (V_{drift_o}/τ_D) are determined through a linear fit to the grounded data, for offset and drift corrections using Eq. 2. For charge accumulation experiments, the SVP is then retracted,

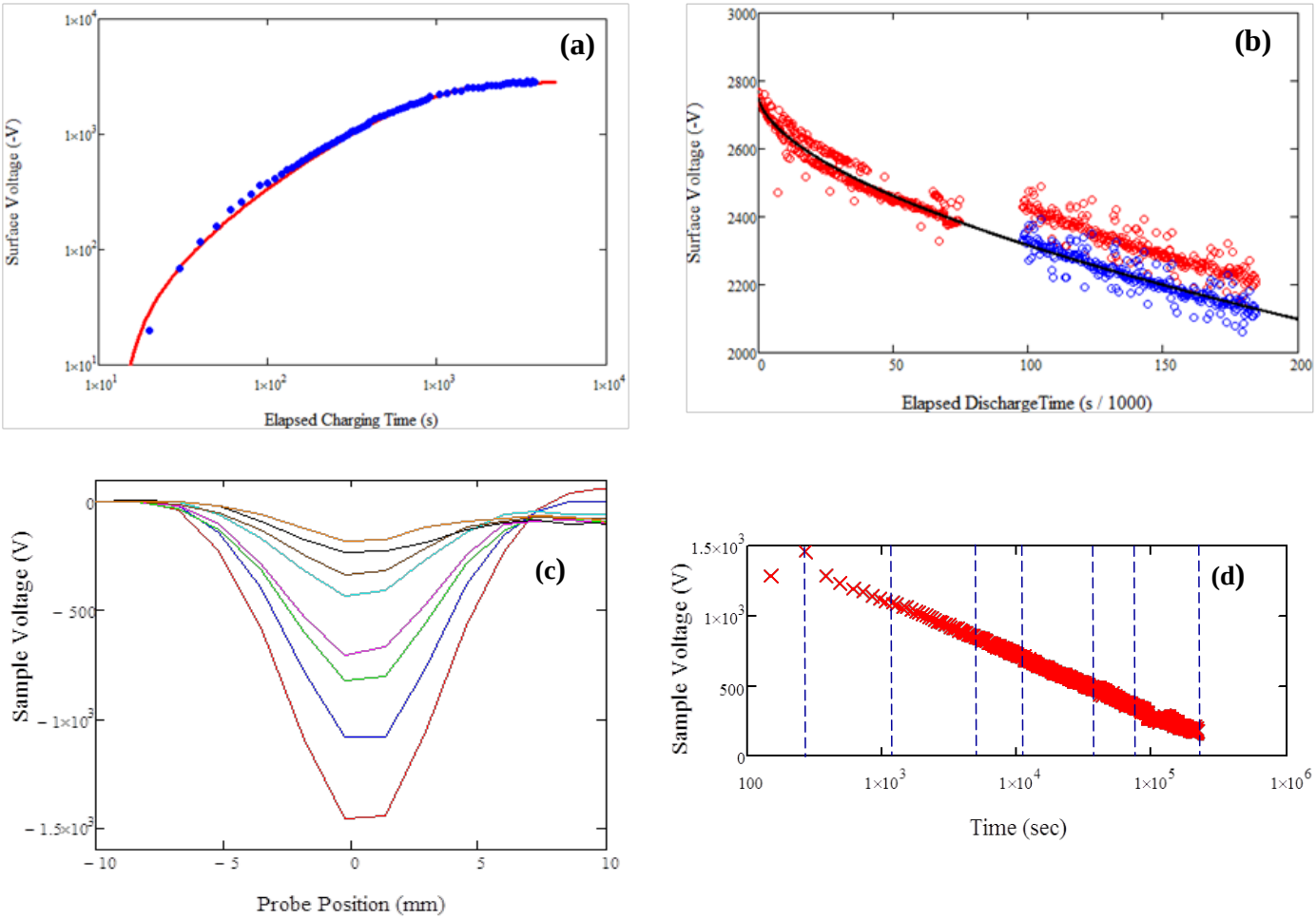

Fig. 5. Surface voltage measurements of Kapton HN™. (a) Charging profile of normalized surface voltage with elapsed time. The fit is based on Eq. (5). (b) Decay curve of normalized surface voltage of a charged polyimide sample. The fit is based on Eq. (4). (c) Decay of radial profile of Kapton HN™ at several times. (Red) 145 s, (Blue) 1169 s, (Green) 5629 s, (Pink) 11040 s, (Cyan) 45640 s, (Brown) 79290 s, (Black) 141200 s, (Orange) 213800 s. Note that the higher voltages for the red and blue curves at right are anomalies due to improper correction for voltage drifts. (d) Peak voltage decay of radial profiles during collection of data in (c) with vertical markers showing the points of radial profile.

and the electron beam is un-blanked for different lengths of time from 10 s to 120 s. 1 s wait times were included after SVP movement to allow dissipation of electronic noise.

IV. Applications

Three types of measurements have been made on the prototypical polymeric spacecraft material, polyimide, to illustrate the research capabilities of the new system [12]. The polyimide sample was a 25 μm thick film of Kapton HN™ from Dupont, with a relative dielectric constant, ε_r, of 3.5 and a total electron yield of Y ~0.32 at 5000 eV. First, using a pulsed electron beam, periodic measurements of the surface voltage were made (see Fig. 5(a)). A total dose of 3 μC-cm^{-2} was delivered over ~60 min. Charge pulse durations were increased from 10 s to 30 s at approximately 340 s of injected charge and then again from 30 s to 120 s at approximately 890 s of injected charge. Second, post charging measurements of the surface voltage were conducted, as deposited charge dissipated to a grounded substrate over a ~50 hr period (see Fig 5(b)). Finally, surface voltage spatial profile measurements were made twice during the charging process and then periodically as the sample discharged to a grounded substrate after exposure (see Fig. 5(c)).

Theoretical models for sample charging and discharge are presented, based on dynamic bulk charge transport equations developed for electron charge carriers to predict the time, temperature, and electric field dependence of the sample net surface voltage [10]. The model includes electron drift, diffusion, and displacement currents and makes direct ties to the interactions between injected electrons, which are trapped in localized states, and the magnitude and energy dependence of the density of those localized trap states within the gap; the carrier mobility, and the carrier trapping and de-trapping rates are then evaluated using the model. An overview of the models is provided in [33], with more details in [10] and [12].

For the experimental conditions considered here, the generalized time-dependant conductivity for non-Ohmic conductivity in highly disordered insulating materials [10] is restricted to : (i) times less than the transit time or $t < (\epsilon_o \epsilon_r / \sigma_{DC})$; (ii) polarization has come to equilibrium before the first decay point is acquired; (iii) persistent radiation induce conductivity (RIC) has dissipated. This leaves

$$\sigma(t) \approx \sigma_o \left\{ 1 + \left[\frac{\sigma^o_{diffusion}}{\sigma_o} \right] t^{-1} + \left[\frac{\sigma^o_{dispersive}}{\sigma_o} \right] t^{-(1-\alpha)} \right\} \quad (3)$$

where σ_o, $\sigma^o_{diffusion}$ and $\sigma^o_{dispersive}$ represent the long-time quasi-equilibrium conductivity, the propagation of the centroid of

the trapped space charge distribution through diffusion or hopping, and the spreading of the distribution in space, respectively. The dispersion parameter, α, is a measure of the width of the energy distribution of trap state below the conduction band edge. These four parameters are determined from simultaneous fits to the charge and discharge data below. We found σ_o~$5\cdot10^{-20}$ $(\Omega\text{-cm})^{-1}$, which is close to independent room temperature dark current conductivity of $1.5\cdot10^{-19}$ $(\Omega\text{-cm})^{-1}$ measured with a constant voltage charge injection method [8] and $1.7\cdot10^{-19}$ $(\Omega\text{-cm})^{-1}$ measured with a charge storage method [28]. $\sigma^o_{diffusion}$ and $\sigma^o_{dispersive}$ were found to be ~$6.4\cdot10^{-15}$ $(\Omega\text{-cm})^{-1}$ and ~$7.9\cdot10^{-17}$ $(\Omega\text{-cm})^{-1}$, respectively. These dominate the conductivity at early times. The value α=0.55 from the fit is reasonable for Kapton, which is believed to have an approximately exponential distribution of state below the conduction bad edge and is in rough agreement with the value estimated by [34].

A. *Charge Decay*

The discharge curve is shown in Figure 5(b). These data are fit with a simple form of the voltage relation that follows from a decaying capacitor model, with a time dependant conductivity, $\sigma(t)$ given by Eq. (3) as

$$V(t) = V_o\, e^{-t\sigma(t)/\epsilon_o\epsilon_r} \approx V_o\left[1-\left(\frac{\sigma_o\, t}{\epsilon_o\epsilon_r}\right)\left\{1+\left[\frac{\sigma^o_{diffusion}}{\sigma_o}\right]t^{-1}+\left[\frac{\sigma^o_{dispersive}}{\sigma_o}\right]t^{-(1-\alpha)}\right\}\right] \quad (4)$$

[35] and [12] showed that this simple model is very nearly the same as a decay model based on simple injection into the band states and bulk charging properties governed by a simplified set of transport equations developed by [36] and [37].

An anomaly in the Kapton HN™ data is seen in the decay curve, two parallel sets of data in Fig. 5(b) at a given time separated by about 10 V to 60 V. This is effect is attributed to a systematic error in instrumentation related to probe positioning. Upon returning to the sample after ground measurements, the largest source of absolute error in SVP results from the repositioning the detector over sample, estimated to be ~±1.0 mm that can be traced to the mechanism for aligning the detector on the sample stage. The radial profiles in Fig. 5(c) show that a difference in 1 mm in position can have as much as an 8% difference in sample voltage. Reproducibility of the probe repositioning has been substantially improved since these data were acquired [33], but this serves to illustrate an important limitation of the system. For example, if errors of ~8% are tolerable, the SVP can be used in an identical manner to charged storage chamber measurement [5,31].

B. *Charge Accumulation*

A similar model for charge accumulation is given by

$$V_s(t)=\left\{\frac{\left[\frac{q_e N_t}{\epsilon_o\epsilon_r}[1\text{-}Y(E_b)]\right]\left[R(E_b)D\left(1-\frac{R(E_b)}{2D}\right)\right]}{\left(\frac{\epsilon_o\epsilon_r}{\sigma_o}\right)\left\{1+\left(\frac{t\,\sigma_o}{\epsilon_o\epsilon_r}\right)\cdot\left[1+\frac{\sigma^o_{diffusion}}{\sigma_o}(t^{-1})+\frac{\sigma^o_{dispersive}}{\sigma_o}(t^{-(1-\alpha)})\right]\right\}}\right\} x\left[\tau_Q\right]\left[1-e^{-\left(\frac{t}{\tau_Q}\right)\left\{1+\left(\frac{t\,\sigma_o}{\epsilon_o\epsilon_r}\right)\left[1+\frac{\sigma^o_{diffusion}}{\sigma_o}(t^{-1})+\frac{\sigma^o_{dispersive}}{\sigma_o}(t^{-(1-\alpha)})\right]\right\}}\right]^{-1} \quad (5)$$

The model includes dissipation of charge through the same three conductivity parameters used in Eq. (4). It also includes the effect of the charge injection using an electron beam through the dependence of the electron emission on accumulated charge. This leads to the addition of an exponential term in Eq. (5), with the parameter τ_Q = 800 s used to model the yield response to charge accumulation [10,21,33]. A simple model for surface voltage (or time) dependence of the yield for negative charging for beam energies greater than the second crossover energy, based on a charging capacitor with time constant, τ_Q, was proposed [21]:

$$[1-Y(t;E_b)] = [1-Y(E_b)]e^{-(Q(t)/\tau_Q)} \quad (6)$$

τ_Q is a time constant for the exponential approach of the yield to unity, as charge is accumulated. The number of available trap states N_t=$5.5\cdot10^{20}$ traps-cm^{-3} is a reasonable value, though somewhat higher than found by [8] and [34]. A simple rate model of the conductivity through a thin film geometry described by [35] is based on detailed studies of carrier dynamics following previous work [38-43]. This more detailed model provides a fit very similar to Eq. (5).

C. *Spatial Profiles and Surface Diffusion*

To estimate the spatial resolution of the system, the spatial profile of a 10.0 mm diameter conducting Au sample (E) uniformly charged to 1000 V was measured by sweeping the 7.0 mm diameter Au voltage sensor electrode (T) over the sample at 1.3 mm increments. A convolution of the circular electrode, estimated as a circular step function, over this charged conductor (also estimated as a circular step function) provides an estimation of the voltage profile. The spatial resolution for the larger diameter probe after deconvolution is estimated to be 1 mm to 2 mm.

An experiment was preformed to measure the time evolution of the non-uniform radial charge profile of a sample irradiated with an electron beam. Measurements are shown in Fig. 5(c) of the charge distribution on a 10.0 mm diameter polyimide sample produced by ~60 s of cumulative irradiation using a well-characterized, focused, Gaussian electron beam with a measured full width at half maximum of 5.6 mm [44]. The initial charge profile ~145 s after charging, along with six subsequent profiles, are shown. After ~60 s of cumulative irradiation, the sample charge reached a maximum peak voltage of –(1456±5) V. The peak voltage values decayed over the following 24 hr period as shown in Fig. 5(d); the surface voltage decay was similar to that observed in the discharge experiment described above.

Initially, the deconvoluted voltage profile was equal to a Gaussian profile with a FWHM of 6.7 mm, approximately 1.1 mm wider than the incident electron beams measured FWHM. Over time the radial charge profile widths observed in Fig. 5(c) did not change, indicating that that charge dissipation through, not across, the sample was the dominate process and that no measurable radial diffusion occurred after the initial profile was measured ~200 s after deposition began. These results suggest that if any diffusion occurred, the majority of the radial diffusion happened during the first ~200 s when the charging of the material was taking place and radiation induced conductivity (RIC) was active in the thin surface layer, where the beam penetrated. The equilibrium value of

RIC while the 5 keV, 1.1 nA/cm^2 beam is on is estimated as σ_{RIC}~3•10^{-14} (Ω-cm)$^{-1}$, using a RIC coefficient of ~6•10^{-18} (Ω-cm-rad/s)$^{-1}$ [45] and a dose rate of ~8•10^3 rad/s up to a range of ~0.5 μm [15]. The average RIC over the time before the first profile is ~40% of the beam on value, after accounting for the beam duty cycle and the hyperbolic decay of persistent RIC with a decay constant of ~ 220 s [36]. A crude estimate of the mean lateral velocity of the charge FWM is $D\cdot(40\%\cdot\sigma_{RIC}/\varepsilon_o\varepsilon_r)\approx$ 1.5μm/s or ~0.7 mm before the first radial profile is taken; this approximate value is ~60% of the observed expansion of the profile, although it is clear that additional measurements and more realistic calculations are required to confirm this hypothesis.

V. Conclusion

This paper described the design of a versatile high sensitivity surface voltage probe system. We have verified that the new system meets the general design parameters as set by the extent of the spacecraft charging problem. The surface voltage probe (SVP) was demonstrated to have ~1 V to >1kV range (>30 kV theoretical) with a resolution of <0.5 V. The response time was found to be about ~1 s and the spatial resolution was ≲1.5 mm. The instrument was successfully applied to three different types of experiments: electron-induced charging, surface discharge, and measurements of spatial profiles and surface diffusion. These experiments were shown to be modeled well by standard theory and consistent with literature values of the materials parameters. The "potential" for the instrument for important applications in spacecraft charging has clearly been demonstrated.

ACKNOWLEDGEMENT

We gratefully acknowledge the fundamental inspiration, useful discussions, and encouragement of Robb Frederickson. Ryan Hoffmann and Neal Nickles were instrumental in developing the HGRFA and other aspects of the electron emission chamber. Prasanna Swaminathan helped in developing the use of the EFTP at USU.

References

[1] D. Hastings, and H. Garrett, *Spacecraft-environment Interactions*, Cambridge University Press, 1996.

[2] A.R. Frederickson, A.,A. Whittlesey and H. Garrett, "Comparing CRRES Internal Discharge Monitor Results with Ground Tests and Published Guidelines," *Proc. of the 7th Spacecraft Charging Techn. Conf.*, 2001.

[3] D. Ferguson, "New Frontiers in Spacecraft Charging," *IEEE Trans. Plasma Sci.*, vol. 40, no. 2, pp. 1-5, Feb. 2012.

[4] J.R. Dennison, C.D. Thomson, J. Kite, V. Zavyalov, J. Corbridge, "Materials Characterization at Utah State University: Facilities and Knowledgebase of Electronic Properties of Materials Applicable to Spacecraft Charging," *Proc. 8th Spacecraft Charging Techn. Conf.*, Huntsville, Alabama, 2003.

[5] A.R. Frederickson and J.R. Dennison, "Measurement of Conductivity and Charge Storage in Insulators Related to Spacecraft Charging," *IEEE Trans. Nuclear Sci.*, Vol. 50, No. 6, December 2003, pp. 2284-2291.

[6] J.R. Dennison, P. Swaminathan, R. Jost, J. Brunson, N. Green and A. R. Frederickson, "Proposed Modifications to Engineering Design Guidelines Related to Resistivity Measurements and Spacecraft Charging," *Proc. 9th Spacecraft Charging Techn. Conf.*, (Epochal Tsukuba, Tsukuba, Japan, April, 2005).

[7] ASTM D 257-99, Standard Test Methods for DC Resistance or Conductance of Insulating Materials, (1999).

[8] J. Brunson, "Measurement of Charge Decay Time and Resistivity of Spacecraft Insulators Using Charge Storage Method and Application to Theoretical Modeling of Charging Behavior of Insulators," PhD Dissertation; Physics Department; Utah State Univ., 2009.

[9] R. Coelho, L. Levy, and D. Sarrail, "Charge decay measurements and injection in insulators," *J. of App. Phys.*, Vol. 22, No. 9, Sept. 1989, pp. 1406-1409.

[10] J.R. Dennison and A.M. Sim, "Unified Density of States Based Model of Electron Transport and Emission of Spacecraft Materials," *Proc.* 12*th Spacecraft Charging Techn. Conf.*, (Kitakyushu, Japan, May, 2012).

[11] J. Dekany, A.M. Sim, J. Brunson, and J.R. Dennison, "Electron Transport Models and Precision Measurements in a Constant Voltage Chamber," *Proc.* 12*th Spacecraft Charging Techn. Conf.*, (Kitakyushu, Japan, May, 2012).

[12] J. L. Hodges, "*In Situ* Measurements of Electron Beam Induced Surface Voltage of Highly Resistive Materials," MS Thesis, Physics Department; Utah State Univ.,2012.

[13]D. C. Ferguson and S. C. Wimberly, "The Best GEO Daytime Spacecraft Charging Index," *51st AIAA Aerospace Sci. Meet.*, Paper AIAA2013-0810, (Grapevine, TX, Jan. 2013).

[14] T. B. Frooninckx, and J. J. Sojka (1992), Solar Cycle Dependence of Spacecraft Charging in Low Earth Orbit, J. Geophys. Res., 97(A3), 2985–2996.

[15] G. Wilson and JR Dennison, "Approximation of Range in Materials as a Function of Incident Electron Energy," *IEEE Trans. on Plasma Sci.*, **40**(2), 305-310 (2012).

[16] NASA Technical Handbook, "Mitigating In-Space Charging Effects —A Guideline," NASA-STD-4002A, 2011.

[17] J.L. Hodges, A.M. Sim, J. Dekany, G. Wilson, A. Evans, and J.R. Dennison "In Situ Surface Voltage Measurements of Layered Dielectrics," *Proc.* 12*th Spacecraft Charging Techn. Conf.*, (Kitakyushu, Japan, May, 2012).

[18] N. Nickles, "The Role of Bandgap in the Secondary Electron Emission of Small Bandgap Semiconductors: Studies of Graphitic Carbon," PhD Dissertation, Physics Dept,. Utah State Univ., 2002.

[19] W.Y. Chang, J.R. Dennison, N. Nickles and R.E. Davies, "Utah State University Ground-based Test Facility for Study of Electronic Properties of Spacecraft Materials," *Proc. 6th Spacecraft Charging Techn. Conf.*, AFRL Science Center, Hanscom Air Force Base, MA, 1999.

[20] C.D. Thomson, V. Zavyalov, J.R. Dennison, "Instrumentation for studies of electron emission and charging from insulators," *Proc. 8th Spacecraft Charging Techn.. Conf., Huntsville, Alabama, 2003.*

[21] C.D. Thomson, "Measurements of the Secondary Electron Emission Properties of Insulators", Ph.D. Dissertation, Physics Dept., Utah State Univ., 2004.

[22] J.R. Dennison, A. Sim and C. D. Thomson, "Evolution of the Electron Yield Curves of Insulators as a Function of Impinging Electron Fluence and Energy," *IEEE Transaction on Plasma Science,* Vol. 34, No. 5, October 2006, pp. 2204-2218.

[23] R. Hoffmann, JR Dennison C. D. Thomson and J. Albresten, "Low-fluence Electron Yields of Highly Insulating Materials" *IEEE Trans. Plasma Sci.*, Vol. 36, No. 5, October 2008, pp. 2238-2245.

[24] I. Krainsky, W. Lundin, W.L. Gordon, and R.W. Hoffman, Secondary Electron Emission Yield Annual Report for Period July 1, 1979 to June 30, 1980, Case Western Reserve Univ., Cleveland, OH, 1980 (unpub.).

[25] J. Dekany, R. H. Johnson, G. Wilson, A. Evans and JR Dennison, "Ultrahigh Vacuum Cryostat System for Extended Low Temperature Space Environment Testing," *Proc.* 12*th Spacecraft Charging Techn. Conf.*, (Kitakyushu, Japan, May, 2012)

[26] R. Davies, "Measurement of Angle-resolved Secondary Electron Spectra," PhD Dissertation, Physics Department; Utah State Univ., 1999.

[27] J. Kite, "Secondary Electron Production and Transport Mechanisms by Measurement of Angle-Energy Resolved Cross Sections of Secondary and Backscattered Electron Emission," PhD Dissertation; Physics Department; Utah State Univ., 2007.

[28] A.R. Frederickson, C. E. Benson and J. F. Bockman, "Measurement of Charge Storage and Leakage in Polyimides," *Nuclear Instrum. and Methods in Phys. Res. B*, 454-60, 2003.

[29] L. Levy, D. Sarrail, and J. M. Siguier, "Conductivity and secondary electron emission properties of dielectrics as required by NASCAP," *3rd European Symp. on Spacecraft Materials in Space Environment*, 1993, pp. 113-123.

[30] P. Swaminathan, "Measurement of Charge Storage Decay Time and Resistivity of Spacecraft Insulators," MS Thesis, Electrical and Computer Engineering Department; Utah State University, 2004.

[31] P. Swaminathan, A. R. Frederickson, J.R. Dennison, A. Sim, J. Brunson, E. Crapo "Comparison Of Classical And Charge Storage Methods For

Determining Conductivity Of Thin Film Insulators," *Proc. 8th Spacecraft Charging Techn. Conf.*, Huntsville, Alabama, October, 2003.
[32] L. Malter, "Anomalous Secondary Electron Emission A New Phenomenon." *Phys. Rev.*,49, 478.1936.
[33] G. Wilson, J.R. Dennison, A. Evans and J. Dekany "Electron Energy Dependent Charging Effects of Multilayered Dielectric Materials" *Proc. 12th Spacecraft Charging Techn. Conf.*, (Kitakyushu, Japan, May, 2012).
[34] R.C.,Weingart, R.H. Barlett, R.S. Lee and W. Hofer, 1972, "X-Ray-Induced Photoconductivity in Dielectric Films," *IEEE Trans. Nuclear Sci.* **19**, 15.
[35] A.M. Sim, "Unified Model of Charge Transport in Insulating Polymeric Materials," PhD Thesis, Dept. Physics, Utah State Univ., Logan, UT, 2013.
[36] Toomer, R. and T. J. Lewis, 1980, "Charge Trapping in Corona-Charge Polyethylene Films," *J. Phys. D: Appl. Physics* **13**, 1343.
[37] A., Aragoneses, J. Mudarra, M. Belana and J.A. Diego, 2008, "Study of Dispersive Mobility in Polyimide by Surface Voltage Decay Measurements," *Polymer* **49**, 2440.
[38] R.H. Walden, 1972, "A Method for the Determination of High-Field Conduction Laws in Insulating Films in the Presence of Charge Trapping," *J. Appl. Phys.* **43**, 1178.
[39] H.J. Wintle, 1973, "Absorption Current, Dielectric Constant, and Dielectric Loss by the Tunneling Mechanism," *J. Appl. Phys.* **44**, 2514.
[40] H.J. Wintle, 1974, "Absorption Currents and Steady Currents in Polymer Dielectrics," *J. Non-Crystalline Solids* **15**, 471.
[41] H.J. Wintle, 1977, "Photoelectric Effects in Insulating Polymers and Their Relation to Conduction Processes," *IEEE Trans. Electrical Insulation* **12**, 97.
[42] D. Liufu, ,X.S. Wang, D.M. Tu and K.C. Kao, 1998, "High-Field Induced Electrical Aging in Polypropylene Films," *J. Phys. D: Appl. Phys.* ***83****, 2209*.
[43] G. Montanari, G. Mazzanti,F. Palmieri, A. Motori, G. Perego and S. Serra, 2001, "Space-Charge Trapping and Conduction in LDPE, HDPE and XLPD," *J. Phys.-D Appl. Phys.* **34**, 2902.
[44] R.C. Hoffmann, "Electron-Induced Electron Yields of Uncharged Insulating Materials," M.S. Thesis, Dept. Physics, Utah State Univ., Logan, UT, 2010.
[45] J.R. Dennison, J. Gillespie, J.L. Hodges, R.C. Hoffmann, J. Abbott, A.W. Hunt and R. Spalding, "Radiation Induced Conductivity of Highly-Insulating Spacecraft Materials," in *Application of Accelerators in Research and Industry*, Am. Instit. Phys. Conf. Proc. Series, Vol. 1099, ed. F.D. McDaniel and B. L. Doyle, (Am. Instit. of Phys., Melveille, NY, 2009), pp. 203-208.

Joshua L. Hodges received a BS in Mechanical Engineering in 2006 and an MS in Physics in 2012 from Utah State University in Logan, UT. He worked with the USU GAS team on the design, construction and pre-flight testing of *SUSpECS* and with the Materials Physics Group on MISSE retrieval and post-flight analysis of *SUSpECS*. He is currently the Service Life Monitoring Program Manager with the T-38 Aircraft Structural Integrity Program at Hill Air Force Base in Ogden, UT.

JR Dennison received the B.S. degree in physics from Appalachian State University, Boone, NC, in 1980, and the M.S. and Ph.D. degrees in physics from Virginia Tech, Blacksburg, VA in 1983 and 1985, respectively. He was a Research Associate with the University of Missouri—Columbia before moving to Utah State University (USU), Logan, UT in 1988. He is currently a Professor of physics at USU, where he leads the Materials Physics Group. He has worked in the area of electron scattering for his entire career and has focused on the electron emission and resistivity of materials related to spacecraft charging for the last two decades.

Justin Dekany is currently a graduate student at Utah State University in Logan, UT pursing an MS in physics. He received a BS degree in physics from USU in 2010. He has worked with the Materials Physics Group for four years on electron transport measurements, electrostatic discharge tests, electron emission measurements, and luminescence studies related to spacecraft charging. He has been the Lab Manager for the Materials Physics Group for the last two years.

Greg Wilson is currently a graduate student at Utah State University in Logan, UT pursing an MS in physics. He received BS degrees in physics and mathematics from USU in 2011. He has worked with the Materials Physics Group for two years on electron emission and luminescence studies related to spacecraft charging. He also developed a composite model for electron range over a wide range of incident energies applicable to diverse materials.

Amberly Evans is currently a graduate student at Utah State University in Logan, UT pursing an MS in physics. She received BS degrees in physics and chemistry from USU in 2012. She has worked with the Materials Physics Group for five years on electron emission, luminescence and resistivity studies and on MISSE retrieval and post-flight analysis of *SUSpECS*. Much of her work has focused on optical scattering and luminescence of spacecraft materials.

Alec Sim is a graduate student at Utah State University in Logan, UT pursing a PhD in physics. He received BS degree in physics from University of California-San Bernardino, CA in 2004 and an MS in physics from University of Kentucky, Lexington, KY in 2008. He has worked with the Materials Physics Group for six years on electron emission measurements and theoretical studies of electron transport in highly disordered insulating materials. He is currently an Assistant Professor in the Department of Physical Sciences at Irvine Valley College, Irving CA.